Monthly Notices of the ROYAL ASTRONOMICAL SOCIETY

MNRAS **428**, 2467–2479 (2013) doi:10.1093/mnras/sts206

The structure of reionization in hierarchical galaxy formation models

Han-Seek Kim,[1★] J. Stuart B. Wyithe,[1,3] Sudhir Raskutti,[1] C. G. Lacey[2] and J. C. Helly[2]

[1]*School of Physics, The University of Melbourne, Parkville, VIC 3010, Australia*
[2]*Institute for Computational Cosmology, Department of Physics, University of Durham, South Road, Durham DH1 3LE*
[3]*ARC Centre of Excellence for All-sky Astrophysics (CAASTRO), Australia*

Accepted 2012 October 13. Received 2012 October 1; in original form 2012 March 15

ABSTRACT

Understanding the epoch of reionization and the properties of the first galaxies represents an important goal for modern cosmology. The structure of reionization and hence the observed power spectrum of redshifted 21-cm fluctuations are known to be sensitive to the astrophysical properties of the galaxies that drove reionization. Thus, detailed measurements of the 21-cm power spectrum and its evolution could lead to measurements of the properties of early galaxies that are otherwise inaccessible. In this paper, we make predictions for the ionized structure during reionization and the 21-cm power spectrum based on detailed models of galaxy formation. We combine the semi-analytic GALFORM model implemented within the Millennium-II dark matter simulation, with a semi-numerical scheme to describe the resulting ionization structure. Semi-analytic models based on the Millennium-II Simulation follow the properties of galaxies within haloes of mass greater than $\sim 1.4 \times 10^8\,\mathrm{M}_\odot$ at $z > 6$, corresponding to the faint sources thought to dominate reionization. Using these models we show that the details of supernovae (SNe) and radiative feedback affect the structure and distribution of ionized regions, and hence the slope and amplitude of the 21-cm power spectrum. These results indicate that forthcoming measurements of the 21-cm power spectrum could be used to uncover details of early galaxy formation. We find that the strength of SN feedback is the dominant effect governing the evolution of structure during reionization. In particular, we show SN feedback to be more important than radiative feedback, the presence of which we find does not influence either the total stellar mass or overall ionizing photon budget. Thus, if SN feedback is effective at suppressing star formation in high-redshift galaxies, we find that photoionization feedback does not lead to self-regulation of the reionization process as has been thought.

Key words: Cosmology: theory – dark ages, reionization, first stars – diffuse radiation – Galaxies: high-redshift.

1 INTRODUCTION

In anticipation of forthcoming 21-cm observations of the epoch of reionization, a great deal of theoretical attention has focused on the prospects of measuring the 21-cm power spectrum. To this end, significant progress has been made in modelling the effect of galaxies on the reionization of the intergalactic medium (IGM). In large modern simulations, the most common approach is to begin with an *N*-body code to generate a distribution of haloes (e.g. Ciardi, Stoehr & White 2003; Sokasian et al. 2003; Iliev et al. 2007; Trac & Cen 2007; Zahn et al. 2007; Iliev et al. 2008; Shin, Trac & Cen 2008; Trac, Cen & Loeb 2008). A simple prescription is then used to relate halo mass to ionizing luminosity. Following this step, radiative transfer methods (most commonly ray-tracing algorithms) are employed to model the generation of ionized structure on large scales. The radiative transfer is normally run with lower resolution than the *N*-body code for computational efficiency.

These simulations describe the generic features of reionization (e.g. Iliev et al. 2007; McQuinn et al. 2007; Zahn et al. 2007; Croft & Altay 2008; Lee et al. 2008; Shin et al. 2008), confirming expectations from analytic models (e.g. Furlanetto, Zaldarriaga & Hernquist 2004a, 2004b; Wyithe & Morales 2007; Barkana 2009) that large-scale, overdense regions near sources are generally reionized first, and that massive galaxies tend to be surrounded by clustered sources that increase the size of H II regions. In addition, the simulations describe the structure of the H II regions, showing that they are generally aspherical (even where the sources are assumed

★E-mail: hansikk@unimelb.edu.au

Published by Oxford University Press on behalf of the Royal Astronomical Society

to emit isotropically). The growth of H II regions during reionization may also be influenced by radiative feedback in the form of suppression of galaxy formation below the cosmological Jeans mass within a heated IGM (Dijkstra et al. 2004), although the importance of this effect remains controversial (Mesinger & Dijkstra 2008). Suppression of low-mass galaxy formation delays and extends the reionization process, which, though started by low-mass galaxies, must then be completed by relatively massive galaxies (Iliev et al. 2007).

An important outcome from the large cosmological volumes attained by modern numerical simulations has been the prediction of 21-cm signals that will be observable using forthcoming low-frequency arrays (e.g. Mellema et al. 2006; Lidz et al. 2008). The most generic features of 21-cm power spectrum modelling were elucidated by Lidz et al. (2008), who show examples of its evolution. On scales of $k \sim 0.1$ Mpc^{-1} the amplitude and the slope of the power spectrum vary in a non-monotonic way relative to the expected shape in the absence of ionization structure. Thus, measurement of the 21-cm power spectrum will provide the first clues regarding the clustering of ionizing sources during reionization. In particular, Lidz et al. (2008) illustrate that the slope and amplitude of the 21-cm power spectrum vary considerably among different models at a given ionization fraction. However, they also find that the behaviour with ionization fraction across the different models is relatively generic. In particular, the amplitude of the 21-cm power spectrum reaches a maximum close to the epoch when ∼50 per cent of the volume of the IGM is ionized, while its slope is found to flatten with increasing ionization fraction. Lidz et al. (2008) argue that first-generation low-frequency radio telescopes like the Murchison Widefield Array (MWA)[1] and the Low-Frequency Array[2] will have sufficient sensitivity to measure the redshift evolution in the slope and amplitude of the 21-cm power spectrum.

One of the main limitations in modelling of reionization is the physics of the ionizing sources. Most studies have used very simple prescriptions to assign ionizing luminosities to dark matter haloes. It has been shown that it is then possible to constrain the parameters for these simple prescriptions. However, an important open question is the degree to which the important astrophysics governing formation and evolution of high-redshift galaxies is accessible via observations of the 21-cm power spectrum. A few studies have previously addressed the issue of realistic modelling of high-redshift galaxies. For example, Raičević, Theuns & Lacey (2011) (see also Benson et al. 2006; Lacey et al. 2011) used the semi-analytical galaxy formation code, GALFORM (Cole et al. 2000; Baugh et al. 2005; Bower et al. 2006), based on Monte Carlo merger trees to evaluate the ionizing photon budget, finding that although galaxies should produce sufficient ionizing photons to complete reionization, most of the galaxies responsible would be below the detection threshold of current surveys. Furthermore, Raičević et al. (2011) and Benson et al. (2006) have studied the effect of supernova (SN) feedback on the global ionizing photon budget and global ionization. However, these studies were restricted to the global evolution, and do not address the ionization structure.

In this paper, we combine detailed models of high-redshift galaxy formation using GALFORM with calculations of the spatial dependence of reionization, and predict the resulting redshifted 21-cm power spectrum. We begin in Section 2 and Section 3 by describing the implementation of GALFORM, and our method for modelling the ionization structure. Then, in Section 4 we present ionization maps for different galaxy formation models, including the effect of SN and radiative feedback. We discuss the ionizing photon budget as a function of halo circular velocity in Section 5, and then present a discussion of the dependence of the 21-cm power spectrum on the galaxy formation model in Section 6. We finish with some conclusions in Section 7.

[1] http://www.haystack.mit.edu/ast/arrays/mwa/

[2] http://www.lofar.org/

2 THE MODEL

In this section we introduce the theoretical galaxy formation modelling used in our analysis. In Section 2.1, we briefly review GALFORM. We then describe the implementations of SNe, active galactic nucleus (AGN) and photoionization feedback processes in Section 2.2.

2.1 The GALFORM galaxy formation model

The formation and evolution of galaxy properties are computed within the Λ cold dark matter (ΛCDM) structure formation framework using the semi-analytical model GALFORM. GALFORM includes a range of processes that are thought to be important for galaxy formation, including (1) the gravitationally driven assembly of dark matter haloes; (2) the density and angular momentum profiles of dark matter and hot gas in haloes; (3) the radiative cooling of gas and its collapse to form centrifugally supported discs; (4) star formation in discs; (5) feedback processes, resulting from the injection of energy from SNe and AGN heating; (6) chemical enrichment of the interstellar medium (ISM) and hot halo gas which affect the gas cooling rate and the properties of the stellar populations in a galaxy; (7) the dynamical friction on orbits of satellite galaxies within a dark matter halo and their possible merger with the central galaxy; (8) the formation of galactic spheroids; (9) the spectrophotometric evolution of stellar populations; (10) the effect of dust extinction on galaxy luminosities and colours, and its dependence on the inclination of a galaxy; and (11) the generation of emission lines from interstellar gas ionized by young hot stars.

A comprehensive overview of GALFORM can be found in Cole et al. (2000), with an updated discussion in the review by Baugh (2006). In this paper, we implement GALFORM within the Millennium-II cosmological *N*-body simulation (Boylan-Kolchin et al. 2009). However, rather than using the halo merger trees presented in Boylan-Kolchin et al. (2009), we base our study on the halo merger trees described in the study of Merson et al. (2012) which are better suited for the purposes of semi-analytic modelling. The simulation has a cosmology including fractional mass and dark energy densities with values of $\Omega_{\rm m} = 0.25$, $\Omega_{\rm b} = 0.045$ and $\Omega_\Lambda = 0.75$, a dimensionless Hubble constant of $h = 0.73$ and a power spectrum normalization of $\sigma_8 = 0.9$. The particle mass of the simulation is $6.89 \times 10^6\, h^{-1}\, {\rm M}_\odot$ and we detect haloes down to 20 particles in the simulation box of side length $L = 100\, h^{-1}$ Mpc.

2.2 Feedback processes

Feedback processes during galaxy formation are very important contributors to the shape of luminosity functions predicted by GALFORM (Cole et al. 2000; Benson et al. 2002; Baugh et al. 2005; Bower et al. 2006; Kim et al. 2011). Three main feedback processes are implemented in GALFORM, which we discuss in turn below.

2.2.1 *SN feedback*

SN feedback on galaxy formation is implemented within GALFORM through the reheating and ejection of cold gas from galaxies via the equation:

$$\dot{M}_{\rm eject} = \beta\psi, \quad (1)$$

where ψ is the instantaneous star formation rate. Here β is the efficiency of the feedback process, parametrized as

$$\beta = (V_{\rm disc}/V_{\rm hot})^{-\alpha_{\rm hot}}, \quad (2)$$

where $V_{\rm hot}$ has unit of km s^{-1}, $\alpha_{\rm hot}$ is a dimensionless adjustable parameter which controls the strength of SN feedback (see Cole et al. 2000) and $V_{\rm disc}$ is the circular velocity of the galactic disc at the half-mass radius. SN feedback suppresses the formation of galaxies within small dark matter haloes, and is required to reproduce the faint end of the observed galaxy luminosity function (e.g. Blanton et al. 2001; Norberg et al. 2002). Bower et al. (2006, hereafter the Bow06 model) adopted values of $V_{\rm hot} = 485$ km s^{-1} and $\alpha_{\rm hot} = 3.2$.

2.2.2 *AGN feedback*

To reproduce the low number density of bright galaxies and the steep slope of the bright end of the galaxy luminosity function, an additional feedback process is needed that operates in the high-mass regime. For this reason, Bow06 included AGN feedback which suppresses the cooling flows in massive haloes. The physical motivation for this lies in the fact that energy is known to be released from accretion of matter on to central supermassive black holes. Bow06 modelled AGN feedback assuming haloes to be in quasi-hydrostatic equilibrium in cases where the cooling time at the cooling radius, $t_{\rm cool}(r_{\rm cool})$, exceeds a multiple of the free-fall time at the cooling radius, $t_{\rm ff}(r_{\rm cool})$, i.e.

$$t_{\rm cool}(r_{\rm cool}) > \frac{1}{\alpha_{\rm cool}} t_{\rm ff}(r_{\rm cool}), \quad (3)$$

where $\alpha_{\rm cool}$ is an adjustable parameter whose value controls the strength of AGN feedback. The value of $\alpha_{\rm cool}$ in the Bow06 model is 0.58. An alternative approach was taken by Baugh et al. (2005, hereafter Bau05) who implemented superwind feedback from star formation with a top-heavy stellar initial mass function (IMF) in order to understand the high-luminosity end of the galaxy luminosity function.

2.2.3 *Photoionization feedback*

In the presence of a strong ionizing background, star formation in small galaxies is quenched owing to several physical processes, including the suppression of cooling by photoheating (Efstathiou 1992), the higher IGM gas pressure (Gnedin 2000) and photoheating (Hoeft et al. 2006; Okamoto, Gao & Theuns 2008). As a result the star formation rate density is suppressed within H II regions during reionization (see Crain et al. 2009), which may result in self-regulation of the reionization process (Iliev et al. 2007). Based on Benson et al. (2002), GALFORM includes a prescription for suppressing the cooling of halo gas on to the galaxy when the IGM becomes globally ionized. In the standard implementation this is assumed to occur at a particular redshift $z_{\rm cut}$. It is assumed that the suppression of cooling occurs when the host halo's circular velocity lies below a threshold value, $V_{\rm cut}$, at redshift $z < z_{\rm cut}$. Rather than a constant $z_{\rm cut}$, in this paper we apply suppression when the cell in which the galaxy resides is fully ionized (see Section 2.3). The adopted value is $V_{\rm cut} = 30$ km s^{-1} for each of the models (Lacey et al. 2011; Lagos et al. 2012). We note that the value of $V_{\rm cut} = 30$ km s^{-1} is used for the Bow06 model in this paper, rather than the original value $V_{\rm cut} = 50$ km s^{-1} used in (Bower et al. 2006).

2.2.4 *Key differences of variant models*

In this paper, we use variants of the GALFORM galaxy formation model described in Section 2.1 based on two main published implementations which we refer to as Bow06 (Bower et al. 2006) and Lagos (Lagos et al. 2012). The Bow06 and Lagos models assume a Kennicutt IMF, similar to that in the solar neighbourhood, for both quiescent star formation and starbursts. The Lagos model is similar to the Bow06 model but it has a new star formation law and has different photoionization feedback parameters. We study three variants of the Bow06 model, in addition to the published version. First, the NOSN model in which we remove SN feedback from the Bow06 model by using a value of $V_{\rm hot} = 0$ km s^{-1}. Second, the Bow06 (no suppression) model in which we remove photoionization by setting $V_{\rm cut} = 0$ km s^{-1}, and third the NOSN (no suppression) model in which we remove both SN and radiative feedback (i.e. $V_{\rm hot} = V_{\rm cut} = 0$ km s^{-1}). In Table 1, we summarize the values of selected parameters for the different models used in this paper.

2.3 Modelling spatial dependence of radiative feedback in GALFORM

Photoionization feedback from reionization is normally modelled in semi-analytic models (including GALFORM) using a single value of $z_{\rm cut}$. However, to investigate the effect of galaxy formation on ionization structure during reionization, we need to improve the photoionizing feedback using a spatially dependent value of $z_{\rm cut}$ that accounts for earlier suppression in regions of the IGM where H II regions first form. Broadly, the process is to run GALFORM to a particular redshift snapshot, perform a calculation of ionization structure and then apply radiative suppression to subsequent galaxy formation inside H II regions with halo circular velocities below $V_{\rm cut}$. GALFORM then evolves the population of galaxies to the next snapshot, where the ionization structure is recomputed. Details of the GALFORM specific implementation are provided in Appendix A.

2.4 The High-redshift galaxy luminosity function

It is important to consider how well the predicted galaxy population represents the galaxies observed to exist at high-redshift. GALFORM models are calibrated to a wealth of data at low redshift. Previously, Lacey et al. (2011) used GALFORM with Monte Carlo merger trees (with no built-in mass resolution limit) to compare model predictions with observed properties of high-redshift galaxies at $z \sim 3$–10. Their modelling was successful in reproducing the high-redshift luminosity function, although with dependence on the model used. In our work we have utilized *N*-body merger trees extracted from the Millennium-II Simulation in order to explicitly include the correlations between galaxy position and overdensity in the IGM. Since the Millennium-II Simulation resolves most of the galaxies responsible for reionization, the model predicts the correct star formation rate density. We show the ultraviolet (UV) luminosity functions at high redshifts in Fig. 1 for the Bow06 model and Lagos model based on the Millennium-II dark matter simulation merger trees. The UV luminosity function using the Millennium-II Simulation merger trees

Table 1. The values of selected parameters which are different in the models. The columns are as follows: (1) the name of the model, (2) the value of the photoionization parameter V_{cut}, (3) the SN feedback parameter, V_{hot}, (4) the IMF of brown dwarfs Υ and (5) comments giving model source or key differences from published models.

	V_{cut}(km s^{-1})	V_{hot}(km s^{-1})	Υ	Comments
Bow06	30	485	1	Bower et al. (2006), V_{cut} value change
Lagos	30	485	1	Lagos et al. (2012)
Bow06 (no suppression)	0	485	1	Bower et al. (2006), no radiative suppression
NOSN	30	0	4	Bower et al. (2006), no SN feedback
NOSN (no suppression)	0	0	4	Bower et al. (2006) No SN feedback and no radiative suppression

is nearly identical to the Monte Carlo merger trees for the Bow06 model (see Lacey et al. 2011). The Bow06 model (solid lines in Fig. 1) agrees well with the observational results, with the exception of an overprediction of luminous galaxies. The Lagos model (dashed lines in Fig. 1) shows better agreement with the data across all redshifts and luminosities. The Lagos model has a different star formation law to the Bow06 model, and adopts a burst time-scale that also gives better agreement with the UV luminosity function at $z \sim 3$–7 following the analysis in the Lacey et al. (2011). Importantly, both models agree well for the faint galaxies thought to be

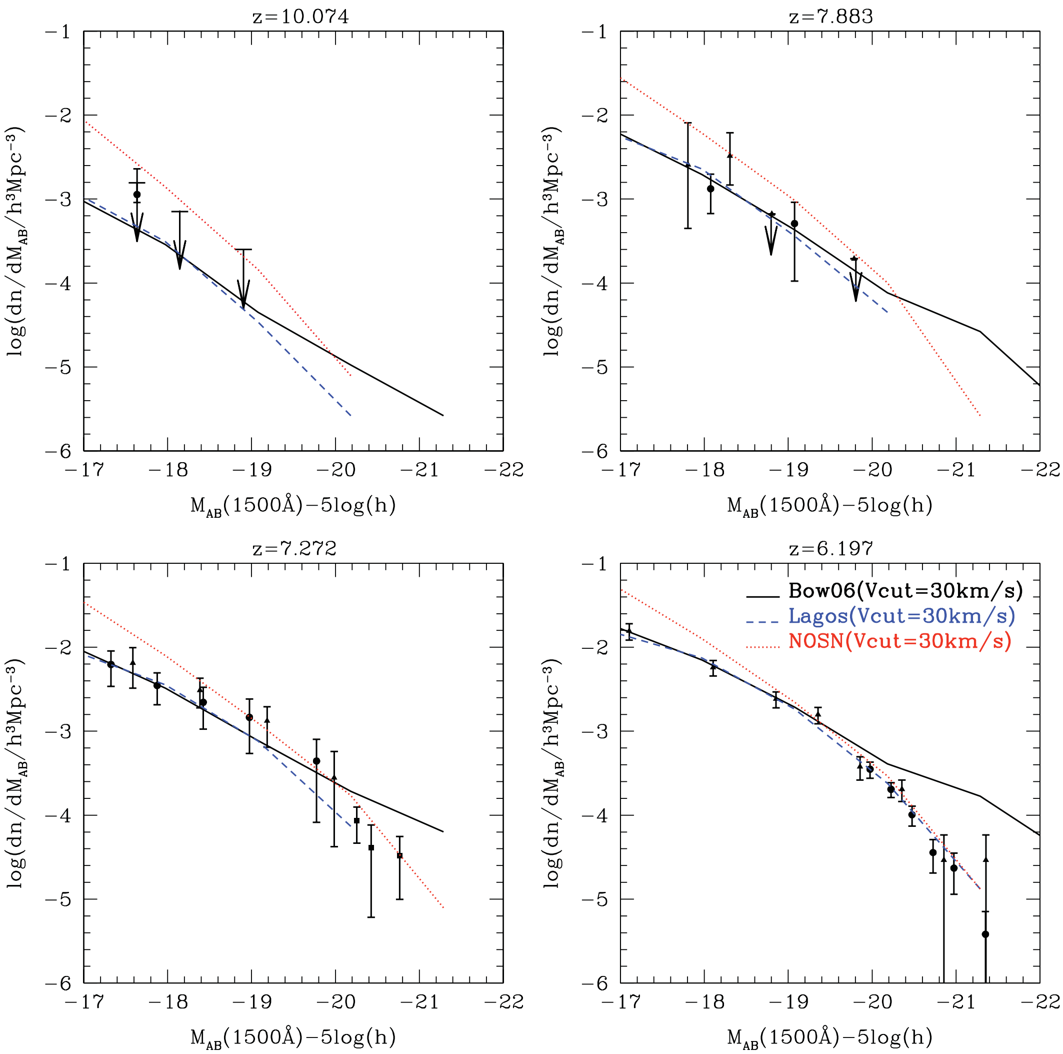

Figure 1. The UV luminosity functions from the Bow06, Lagos and NOSN models with observed data points. The top left-hand panel shows the predicted UV luminosity functions from the models at $z = 10.074$ with the observations estimated by Bouwens et al. (2011) (circle and 1σ upper limit arrows, 1600 Å) for $z \sim 10$. The top right-hand panel shows the $z = 7.883$ predictions from the models including the observations for the $z \sim 8$ measured by Bouwens et al. (2010) (triangles, 1700 Å) and McLure et al. (2010) (circles, 1500 Å). The bottom left-hand panel is the predictions for $z = 7.272$ from models with the observations for $z \sim 7$ came from McLure et al. (2010) (circles, 1500 Å), Oesch et al. (2010) (triangles, 1600 Å) and Ouchi et al. (2010) (squares, 1500 Å). The bottom right-hand panel is for $z = 6.197$ predictions with the observations for $z \sim 6$ measured by McLure et al. (2009) (circles, 1500 Å) and Bouwens et al. (2007) (triangles, 1350 Å).

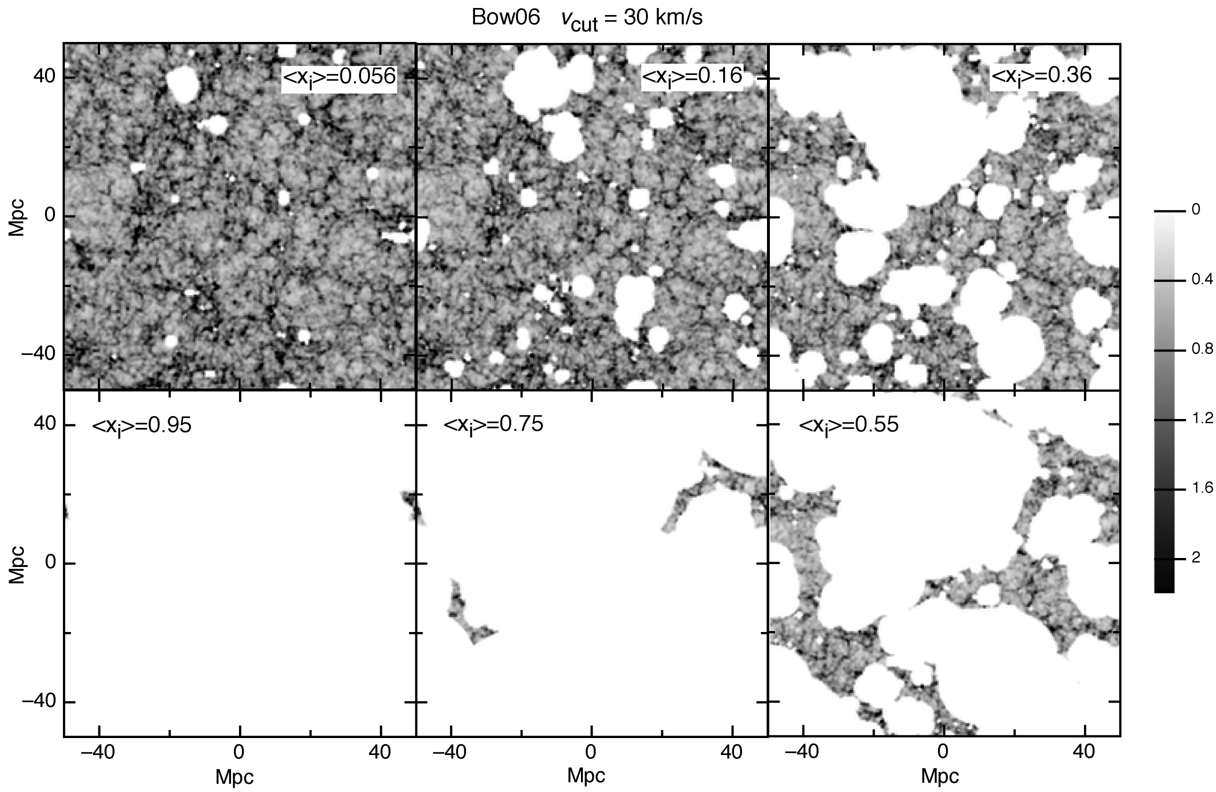

Figure 2. Maps of the 21-cm intensity in slices for a range of values of $\langle x_i \rangle$ corresponding to different stages of reionization. We assume the Bow06 model. The units of the grey scale are $(28[(1+z)/10]$ mK). The slices are 0.3906 h^{-1} Mpc deep.

responsible for reionization, indicating that our results should not be very sensitive to this choice.

We also show the NOSN model. Simply removing the feedback strength of SNe (by setting $V_{\rm hot} = 0$) results in a model which greatly overpredicts the number of galaxies at all luminosities. In order to correct for this we therefore modify the parameter in GALFORM which specifies the ratio between the sum of the mass in visible stars and brown dwarfs, and the mass in visible stars. This parameter (Υ) quantifies the assumption for the IMF of brown dwarfs ($m < 0.1\,{\rm M}_{\odot}$), which contribute mass but no light to stellar population. We adopt a value of $\Upsilon = 4$ for the NOSN and NOSN (no suppression) models. The value of Υ should be greater than unity by definition.

3 SEMI-NUMERICAL SCHEME TO CALCULATE THE EVOLUTION OF IONIZED STRUCTURE

Mesinger & Furlanetto (2007) introduced an approximate but efficient method for simulating the reionization process. This so-called *semi-numerical* method extends prior work by Bond & Myers (1996) and Zahn et al. (2007). The method generates an estimate of the ionization field based on a catalogue of sources assigned within the halo field by applying a filtering technique. Good agreement is found with numerical simulations, implying that semi-numerical models can be used to explore a large range of reionization scenarios. In this paper we apply a semi-numerical technique to find the ionization structure resulting from GALFORM galaxies within the Millennium-II dark matter simulation.

3.1 H II regions

We begin by binning galaxies from the GALFORM model into small regions of volume (or cells). We assume the number of photons produced by galaxies in the cell that enter the IGM and participate in reionization to be

$$N_{\gamma,\rm cell} = f_{\rm esc} \int_0^{t_z} \dot{N}_{\rm Lyc,cell}(t)\,{\rm d}t, \tag{4}$$

where $f_{\rm esc}$ is the escape fraction of photons produced by stars in a galaxy. The total Lyman continuum luminosity of the $N_{\rm cell}$ galaxies within the cell expressed as the emission rate of ionizing photons (i.e. units of photons s^{-1}) computed from GALFORM is

$$\dot{N}_{\rm Lyc,cell}(t) = \sum_{i=1}^{N_{\rm cell}} \dot{N}_{{\rm Lyc},i}(t), \tag{5}$$

where

$$\dot{N}_{{\rm Lyc},i}(t) = \int_{\nu_{\rm thresh}}^{\infty} \frac{L_{\nu,i}(t)}{h\nu}{\rm d}\nu, \tag{6}$$

$L_{\nu,\,i}$ is the spectral energy distribution of galaxy i and $\nu_{\rm thresh}$ is the Lyman-limit frequency, $h\nu_{\rm thresh} = 13.6$ eV. Note that the number of photons produced per baryon in long-lived stars and stellar remnants depends on the IMF and metallicity (Z). The stellar population models used in GALFORM output give 4.54×10^3 for $Z = 0.02$ and 6.77×10^3 for $Z = 0.004$ using the Kennicutt IMF. Note that we assume the total Lyman continuum luminosity in a cell at redshift z_i to be constant until the next snapshot at redshift z_{i+1}, and calculate the number of photons produced in the cell between z_i and z_{i+1} to be $\dot{N}_{\rm Lyc,cell}(t_{z_i}) \times (t_{z_{i+1}} - t_{z_i})$.

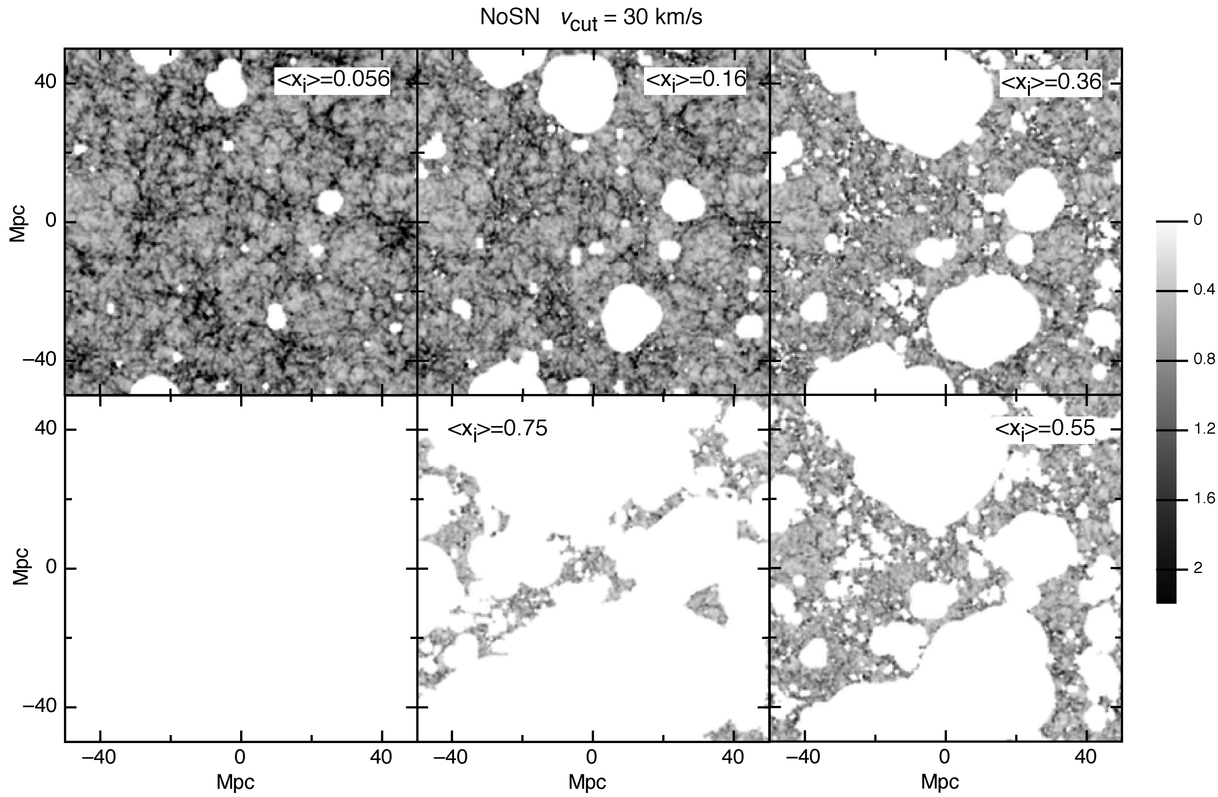

Figure 3. Maps of the 21-cm intensity in slices for a range of values of $\langle x_i \rangle$ corresponding to different stages of reionization. We assume the NOSN model. The units of the grey scale are $(28[(1+z)/10]$ mK). The slices are 0.3906 h^{-1} Mpc deep.

We then calculate the ionization fraction within each cell according to

$$Q_{\rm cell} = \left[\frac{N_{\gamma,\rm cell}}{(1+F_{\rm c})N_{\rm HI,cell}}\right], \quad (7)$$

where $F_{\rm c}$ denotes the mean number of recombinations per hydrogen atom up to reionization and $N_{\rm HI,\,cell}$ is the number of neutral hydrogen atoms within a cell. The latter quantity is calculated as

$$N_{\rm HI,cell} = n_{\rm HI}(\delta_{\rm DM,cell}+1)V_{\rm cell}, \quad (8)$$

where we assume that the overdensity of neutral hydrogen follows the dark matter (computed based on the Millennium-II Simulation density field), $n_{\rm HI}$ is the mean comoving number density of hydrogen atoms and $V_{\rm cell}$ is the comoving volume of the cell. Self-reionization of a cell occurs when $Q_{\rm cell} = 1$. We divide the Millennium-II Simulation box into 256^3 cells, yielding cell side lengths of 0.3906 h^{-1} Mpc and comoving volumes of 0.0596 h^{-3} Mpc^3.

Theoretical prediction of the parameters $F_{\rm c}$ and $f_{\rm esc}$ in equations (4) and (7) is complicated, and their values are not known. The recombination parameter $F_{\rm c}$ is related to the density of the IGM on small scales, while $f_{\rm esc}$ depends on the details of the high-redshift ISM. Previous work using GALFORM suggested the value $(1+F_{\rm c})/f_{\rm esc} \sim 10$ (Benson et al. 2001; Raičević et al. 2011) to fit observational constraints on reionization. Here, we determine the value of $(1+F_{\rm c})/f_{\rm esc}$ that is required in order to give a particular value of ionization fraction at each redshift. We explicitly note here our assumption that values of $(1+F_{\rm c})/f_{\rm esc}$ do not depend on galaxy mass. In reality the escape fraction may be mass dependent, particularly in models with SN feedback.

Based on equation (7), individual cells can have $Q_{\rm cell} > 1$. On the other hand, cells with $Q_{\rm cell} < 1$ may be ionized by photons produced in a neighbouring cell. In order to find the extent of ionized regions we therefore filter the $Q_{\rm cell}$ field using a sequence of real-space top-hat filters of radius R (with $0.3906 < R < 100\,h^{-1}$ Mpc), producing one smoothed ionization field Q_R per radius. At each point in the simulation box we find the largest R for which the filtered ionization field is greater than unity (i.e. ionized with $Q_R > 1$). All points within the radius R around this point are considered ionized. This procedure forms the position-dependent ionization fraction $0 \le Q \le 1$, which describes the ionization structure of the IGM during reionization. The filtering follows the method outlined in more detail in Geil & Wyithe (2008).

3.2 Redshifted 21-cm intensity

Fluctuations in 21-cm intensity (or brightness temperature) from different regions of the IGM include contributions from a range of different physical properties, including density, velocity gradients, gas temperature, hydrogen spin temperature and ionization state (Furlanetto, Oh & Briggs 2006). In this paper we restrict our attention to analyses that assume that the spin temperature of hydrogen is coupled to the kinetic temperature of an IGM that has been heated well above the cosmic microwave background (CMB) temperature (i.e. $T_{\rm s} \gg T_{\rm CMB}$). This condition should hold during the later stages of the reionization era ($z \lesssim 9$; Santos et al. 2008). In this regime there is a proportionality between the ionization fraction and 21-cm intensity, and the 21-cm brightness temperature contrast may be written as

$$\Delta T = 23.8\left(\frac{1+z}{10}\right)^{1/2}[1-Q]\left(1+\delta_{\rm DM,cell}\right)\ {\rm mK}. \quad (9)$$

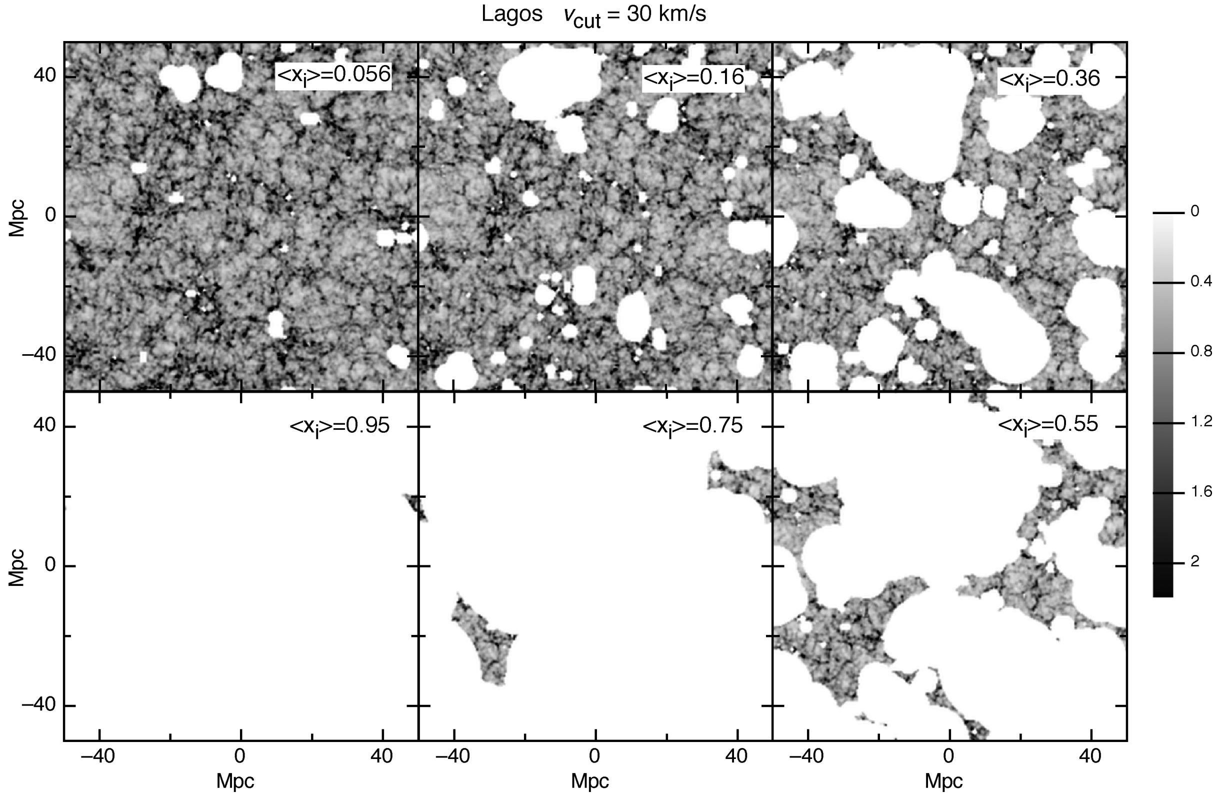

Figure 4. Maps of the 21-cm intensity in slices for a range of values of $\langle x_i \rangle$ corresponding to different stages of reionization. We assume the Lagos model. The units of the grey scale are $(28[(1 + z)/10]$ mK). The slices are 0.3906 h^{-1} Mpc deep.

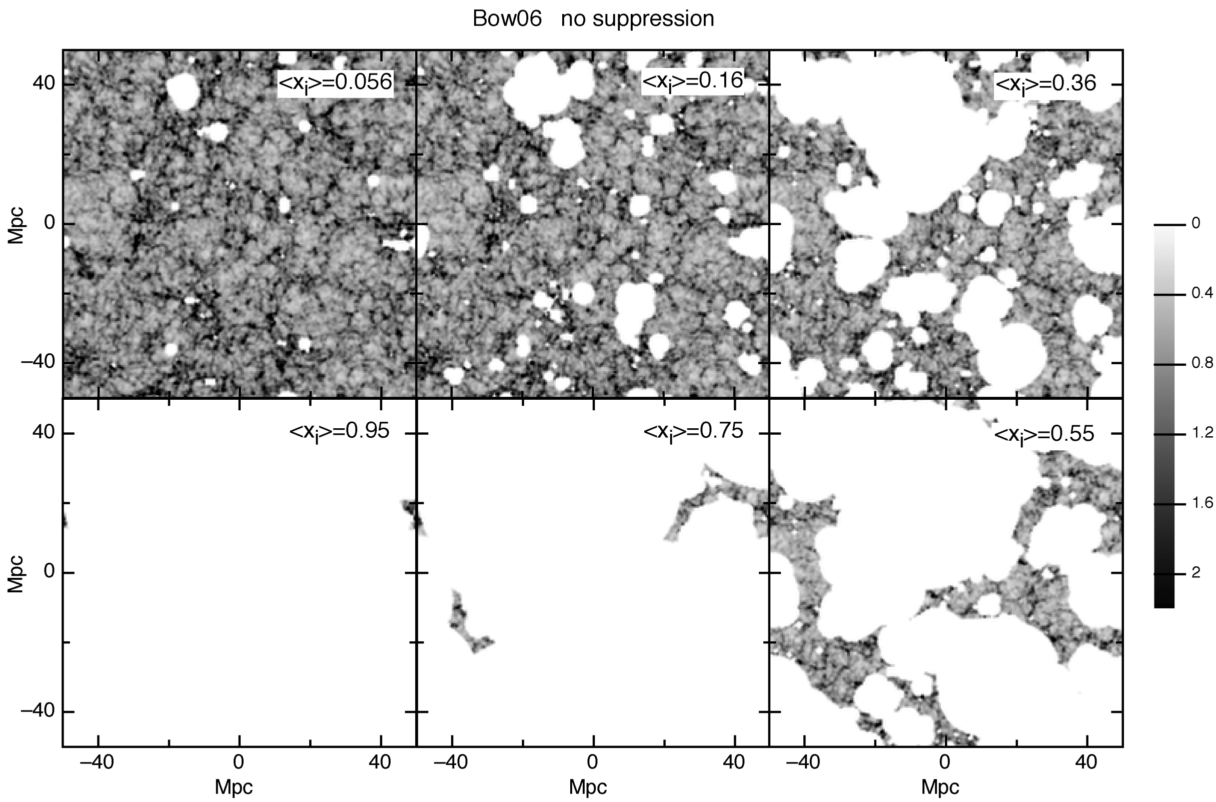

Figure 5. Ionization maps for a range of values of $\langle x_i \rangle$ corresponding to different stages of reionization. We assume the Bow06 (no suppression) model. The units of the grey scale are $(28[(1 + z)/10]$ mK). The slices are 0.3906 h^{-1} Mpc deep.

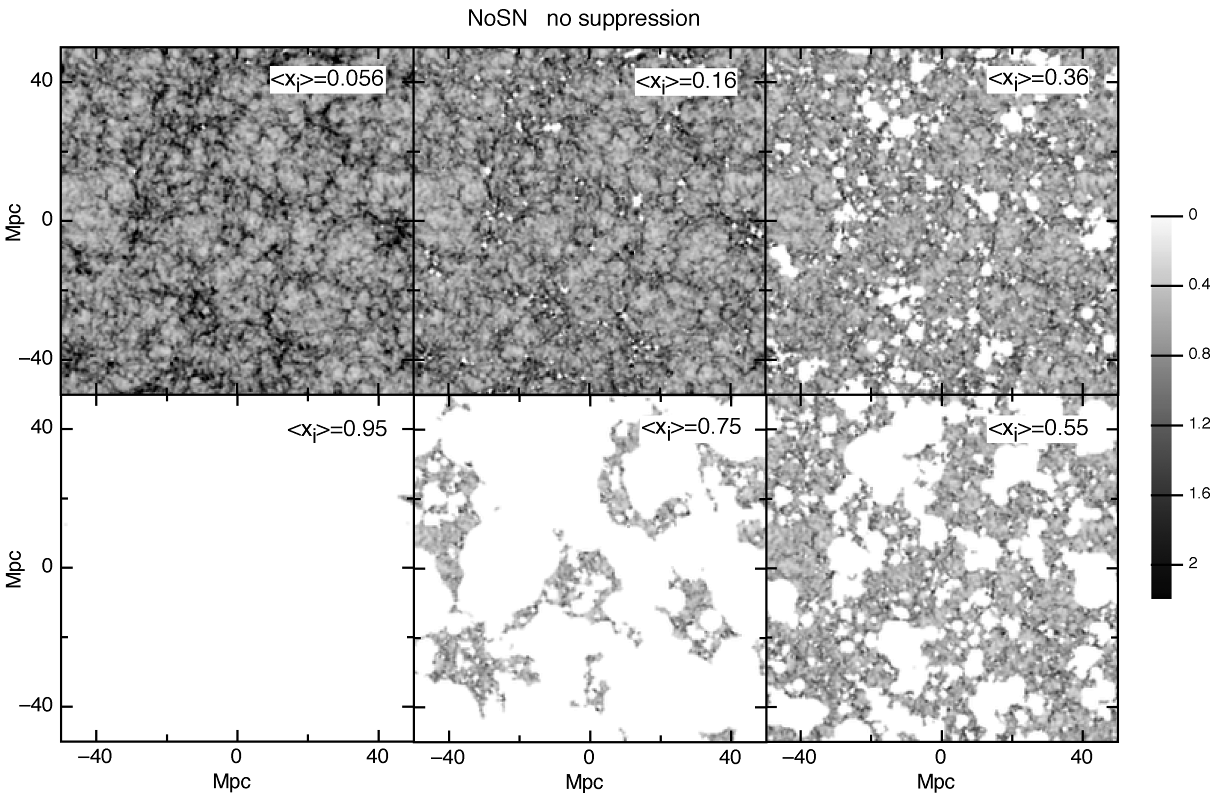

Figure 6. Ionization maps for a range of values of $\langle x_i \rangle$ corresponding to different stages of reionization. We assume the NOSN (no suppression) model. The units of the grey scale are $(28[(1+z)/10]$ mK). The slices are 0.3906 h^{-1} Mpc deep.

Here we have ignored the contribution to the amplitude from velocity gradients, and assumed as before that the hydrogen overdensity follows the dark matter ($\delta_{\rm DM,\,cell}$).

4 STRUCTURE OF REIONIZATION

In this section we present results for the possible structure of ionization in the IGM. In Figs 2–6, we show example ionization maps for our five different models. In each case we show examples for $\langle x_i \rangle = 0.95$, 0.75, 0.55, 0.36, 0.16 and 0.056, illustrating the growth of H II regions during reionization. For our model these values correspond to redshifts of $z \sim 6.197$, 6.712, 7.272, 7.883, 8.550 and 9.278 (selected for comparison with the work by Lidz et al. 2008). Maps are shown for Bow06, NOSN and Lagos models in Figs 2–4, and for Bow06 (no suppression) and NOSN (no suppression) models in Figs 5 and 6. In order to make this comparison we adjust the quantity $(1 + F_c)/f_{\rm esc}$ in equations (4) and (7) so as to get same mass-averaged ionization fraction $\langle x_i \rangle$ for all models at each redshift. The values of $(1 + F_{\rm c})/f_{\rm esc}$ required in order to give a particular values of ionization fraction at each redshift are shown in Table 2. Models presented in this work take values of $(1 + F_{\rm c})/f_{\rm esc}$ that are less than 10 for models including SN feedback in agreement with the work of Benson et al. (2001) and Raičević et al. (2011), but greater than 50 for models without SN feedback.

The effects of SN feedback strength (between the Bow06 model and the NOSN model) and of star formation law (between the Bow06 model and the Lagos model) on the ionization history can be seen explicitly by comparing Figs 3 and 4 with Fig. 2. The regulation of star formation and cooling of hot gas in small galaxies by the SN feedback process leads to massive galaxies which are more biased towards dense regions, dominating the production of ionizing photons. As a result, the evolution of large H II regions in the Bow06 model (Figs 2) starts from the overdense environment and propagates to neighbouring overdense regions. Conversely, the production of ionization photons from the massive galaxies is less prominent in the NOSN model (Fig. 3) than in the Bow06 model. As a result the H II region evolution maps for the NOSN model show many more smaller H II regions than in the Bow06 case. The

Table 2. The values of $(1 + F_{\rm c})/f_{\rm esc}$ corresponding to the different models and redshifts shown in this paper.

Redshift (z)	9.278	8.550	7.883	7.272	6.712	6.197
$\langle x_i \rangle$	0.056	0.16	0.36	0.55	0.75	0.95
Bow06	4.85	3.24	2.72	3.10	3.83	4.82
Bow06 (no suppression)	4.856	3.24	2.71	3.12	3.85	4.81
Lagos	3.86	2.61	2.17	2.53	3.11	3.95
NOSN	417.98	189.28	106.70	85.59	74.83	68.94
NOSN (no suppression)	267.78	136.97	85.03	73.86	69.62	68.28

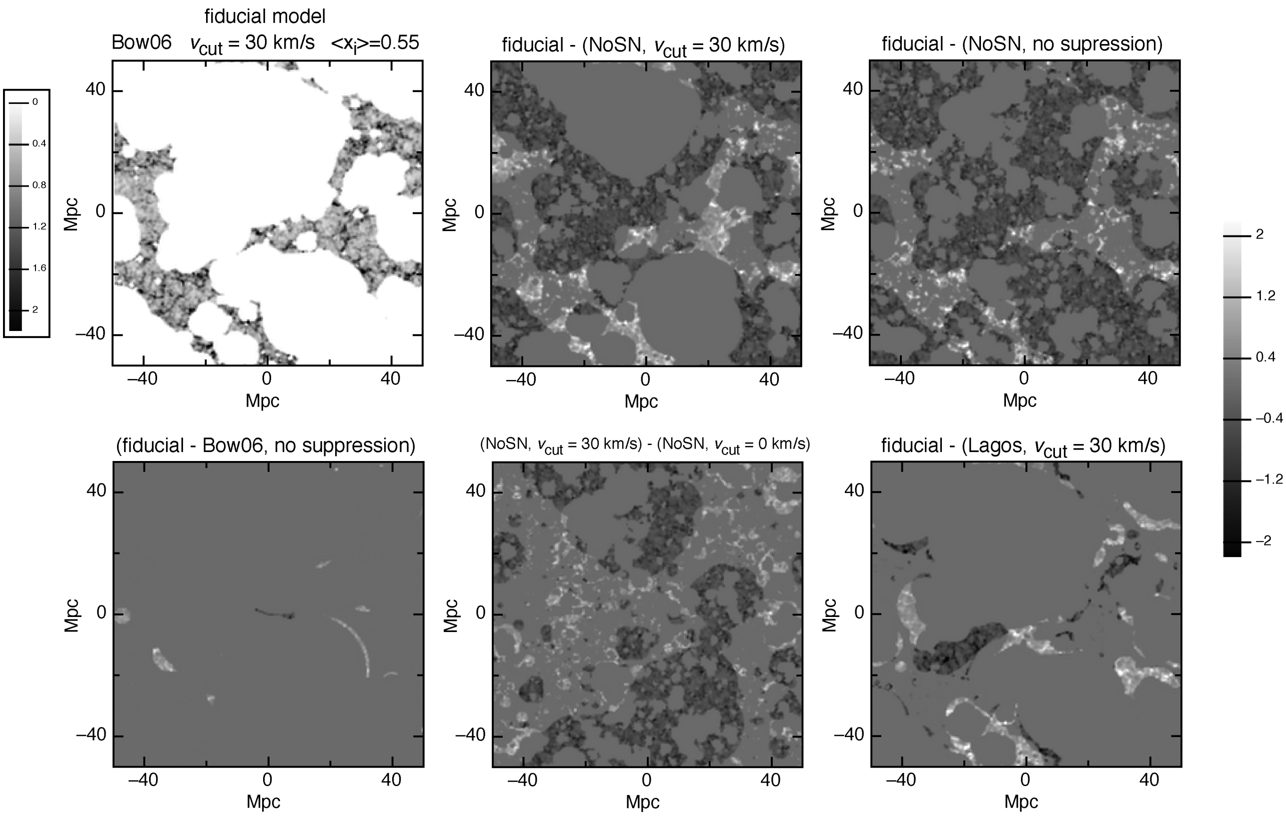

Figure 7. Example maps of the ionization structure produced by our modelling. In each case the slices shown are 100 h^{-1} Mpc on a side and 0.3906 h^{-1} Mpc deep. The models were computed with $\langle x_i \rangle = 0.55$ ($z = 7.272$). The top left-hand panel shows map for the Bow06 model. To make the effect of SNe and photoionization feedback on the ionization map clear, the others show the subtraction of the Bow06 map from the variant model's maps except the bottom middle panel. Here a positive value shows regions where the Bow06 model predicts H II region but variant models do not. Conversely the negative values show regions where the variant models predict ionization but the Bow06 model does not. The units of the grey scale are $(28[(1+z)/10]$ mK).

different star formation law prescriptions in the Lagos (Fig. 4) and Bow06 models also lead to differences in evolution of H II regions. However, the variation is much smaller than is found from differences in the SN feedback strength.

The effect of photoionization feedback on the H II regions evolution can be seen by comparing Figs 5 and 6 with Fig. 2. We find very little difference between the H II region evolution in the Bow06 model and the Bow06 (no suppression) model (Fig. 5). Thus, the effect of SN feedback on the evolution of ionization structure is much larger than that from photoionization feedback. However, in the absence of SN feedback, the effect of photoionization feedback effect is significant (Fig. 6), and the NOSN (no suppression) model produces numerous, smaller H II regions that are relatively homogeneously distributed through the IGM.

To highlight the differences between the maps produced by models with and without SN and/or photoionization feedback, in Fig. 7 we show differences between ionization maps for the Bow06 and other models. The exception is the lower middle panel, which shows the difference between maps for the NOSN and NOSN (no suppression) models. In all cases the mass-averaged ionization fraction is $\langle x_i \rangle = 0.55$ ($z = 7.272$). Positive values represent the area where the Bow06 model predicts H II regions but alternative models do not [in the lower middle panel the positive values represent the area where the NOSN model predicts H II regions but the NOSN (no suppression) does not]. This figure clearly shows the large effect of SN feedback relative to photoionization feedback and star formation prescription.

5 CONTRIBUTIONS TO THE IONIZING PHOTON BUDGET

Radiative feedback has been thought to play a significant role in self-regulating the reionization process by suppressing galaxy formation in reionized regions (e.g. Iliev et al. 2007). These studies were based on the assumption that the ionizing luminosity to halo mass ratio does not depend on halo mass. However, the presence of SN feedback in galaxy formation models is known to modify the mass-to-light ratio of galaxies through regulation of star formation. Motivated by the unexpectedly small difference in ionizing structure between models with SN feedback that do and do not include radiative feedback, in this section we calculate the effect of radiative feedback on stellar mass and ionizing photon contribution.

First, in Fig. 8, we show the cumulative fraction of stellar mass as a function of $V_{\rm halo}$ (km s^{-1}) at $\langle x_i \rangle = 0.55$ for the Bow06 (no suppression) and the NOSN (no suppression) models. The contribution to total stellar mass from galaxies which have circular velocities $V_{\rm halo}$ smaller than 30 km s^{-1} (left dotted line) is almost zero for the Bow06 (no suppression) model and 25 per cent for the NOSN (no suppression) model. This shows that SN feedback greatly lowers the potential contribution of low circular velocity galaxies, which are the ones affected by the photoionization feedback process, and explains why SN feedback is the more dominant effect.

Similarly, we also calculate the fraction $F_{N_{\rm photons}}$ of ionizing photons produced by galaxies with $V_{\rm halo}$ less than 30 km s^{-1} for the Bow06 (no suppression) and the NOSN (no suppression) models.

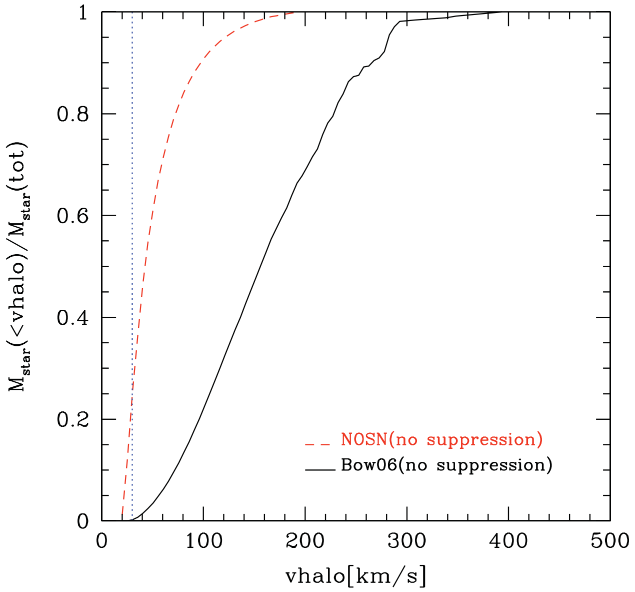

Figure 8. The cumulative fraction of stellar mass as a function of $V_{\rm halo}$(km s^{-1}) at $\langle x_i \rangle = 0.55$ (corresponding to $z = 7.272$) for the NOSN (no suppression) and Bow06 (no suppression) models. The vertical line indicates the value of $V_{\rm cut} = 30$ km s^{-1}.

Table 3. The values of $F_{N_{\rm photons}}$, the fraction of ionizing photons where the galaxy circular velocity less than 30 km s^{-1}.

Model	$V_{\rm halo}$ <30 km s^{-1}	All
Bow06 (no suppression)	0.0028	1
NOSN (no suppression)	0.39	1

The values are listed in Table 3, and show the small fraction of photons produced by the low-mass haloes which are subject to the radiative feedback process; see also Raičević et al. (2011) for similar discussion. Thus, we find that SN feedback renders the effect of radiative feedback on the reionization history negligible, indicating that reionization is not self-regulating, as indicated in previous work (e.g. Iliev et al. 2007).

While the calculations presented above provide the quantitative estimate of the effect of SN feedback on the photon budget, we can also provide a simple argument to show qualitatively why SN feedback should be the dominant process governing the contribution of low-mass galaxies to reionization (e.g. Benson et al. 2006; Raičević et al. 2011). Ignoring photoionization feedback ($V_{\rm cut} = 0$), gas cooling is very efficient in haloes with a virial temperature of $T_{\rm vir} \sim 10^4$–10^5 K. We assume that the resulting star formation timescale is shorter than the Hubble time, in which case all of the cooled gas will either form stars or be ejected by SN feedback (equation 2), yielding

$$(1 - R + \beta)M_\star \sim M_{\rm b}, \quad (10)$$

where $M_\star$ is the mass of stars formed (before recycling), $0 < R < 1$ is the recycled fraction and $M_{\rm b}$ is the total mass of baryons in a halo of mass $M_{\rm halo}$. For low-mass galaxies (with $V_{\rm cut} \sim 30$ km s^{-1}) $\beta \gg 1$, and the fraction of baryons converted into stars is $M_\star/M_{\rm b} \sim 1/\beta \sim 10^{-3}\,(V_{\rm halo}/30\,{\rm km\,s^{-1}})^3 \propto M_{\rm halo}$. The total ionizing contribution to reionization is proportional to the product of this fraction and the mass in dark matter haloes [i.e. $(M_\star/M_{\rm b})M_{\rm halo} \propto M_{\rm halo}^2$]. At low masses the halo mass function (number density per unit mass) is $dn/dM_{\rm halo} \propto M_{\rm halo}^{-\gamma}$, with $\gamma \approx 2$. The mass in stars per logarithm of halo mass per unit volume in the Universe is therefore proportional to $M_{\rm halo}^2 \times M_{\rm halo} dn/dM_{\rm halo} \propto M_{\rm halo}$. Thus, we find that very low mass galaxies should contribute little to reionization (see also Wyithe & Loeb 2012).

6 THE 21-CM POWER SPECTRUM

The filtering procedure described in Section 3 provides a three-dimensional map of the ionization structure within the Millennium-II Simulation box, which provides a three-dimensional 21-cm intensity cube via equation (9). From this cube we calculate the dimensionless 21-cm power spectrum

$$\Delta^2(k) = k^3/(2\pi^2)P_{21}(k) \quad (11)$$

as a function of spatial frequency k, where $P_{21}(k)$ is the 21-cm power spectrum. When calculating the power spectrum, velocity gradients increase the amplitude of the spherically averaged redshift space power spectrum by a factor of 4/3 relative to the real-space power spectrum based on linear theory (Barkana & Loeb 2005). Mao et al. (2012) show that this factor can be much higher than 4/3 over the intermediate range $k \sim 0.1 - 1h$/Mpc at the epoch where the IGM is 50 per cent ionized.

The results of Figs 2–6 indicate that the 21-cm power spectrum will depend on the galaxy formation model assumed. This is shown in Fig. 9 which displays power spectra for each of the semi-analytic models in Table 1. From this figure we see that the Bow06 and NOSN models show a large variation in 21-cm power spectrum predictions, with the amplitude of 21-cm power spectrum for the Bow06 model being higher than the NOSN model across all wavenumbers (with the exception of very late in the reionization process). Secondly, the Bow06 and Lagos models show slightly different 21-cm power spectrum predictions. This is because the modified star formation law in the Lagos model relative to the Bow06 model leads to different predictions for the number of luminous galaxies (Fig. 1) and hence the clustering of the ionizing source population. Thirdly, the NOSN model has a larger amplitude for the 21-cm power spectrum than does the NOSN (no suppression) model. This shows that the photoionization effect on the 21-cm power spectrum can be seen in the no SN feedback models. Conversely, we find negligible difference between the Bow06 and Bow06 (no suppression) models. This very small difference means that photoionization feedback can only affect the reionization signature in the absence of SN feedback. These findings represent the main results of the paper.

Fig. 9 also shows the evolution of predicted 21-cm dimensionless power spectra for the different models. The evolution of the power spectrum in Bow06, Bow06 (no suppression) and Lagos models show the characteristic rise and fall described in detail by Lidz et al. (2008). The maximum amplitude of the 21-cm power spectrum occurs at a scale of around $k \sim 0.2\,h^{-1}$ Mpc for an ionization fraction of $\langle x_i \rangle \sim 0.75$. In all models there is a trend for the wavenumber k at which the shoulder due H II regions occurs to decrease (corresponding to increasing size of H II regions) with increasing ionization fraction. The largest difference is seen between the Bow06 and NOSN models, and is most pronounced at large scales (i.e. small wavenumbers). In this regime the NOSN power spectrum is lower than for Bow06. At smaller wavenumbers (i.e. large scales) the Bow06 model has higher amplitude than the NOSN model for all ionization fraction ranges. The difference in amplitude between the two models increases from $\langle x_i \rangle \sim 0.056$ to $\langle x_i \rangle \sim 0.16$, before decreasing later in the reionization history. We cannot distinguish

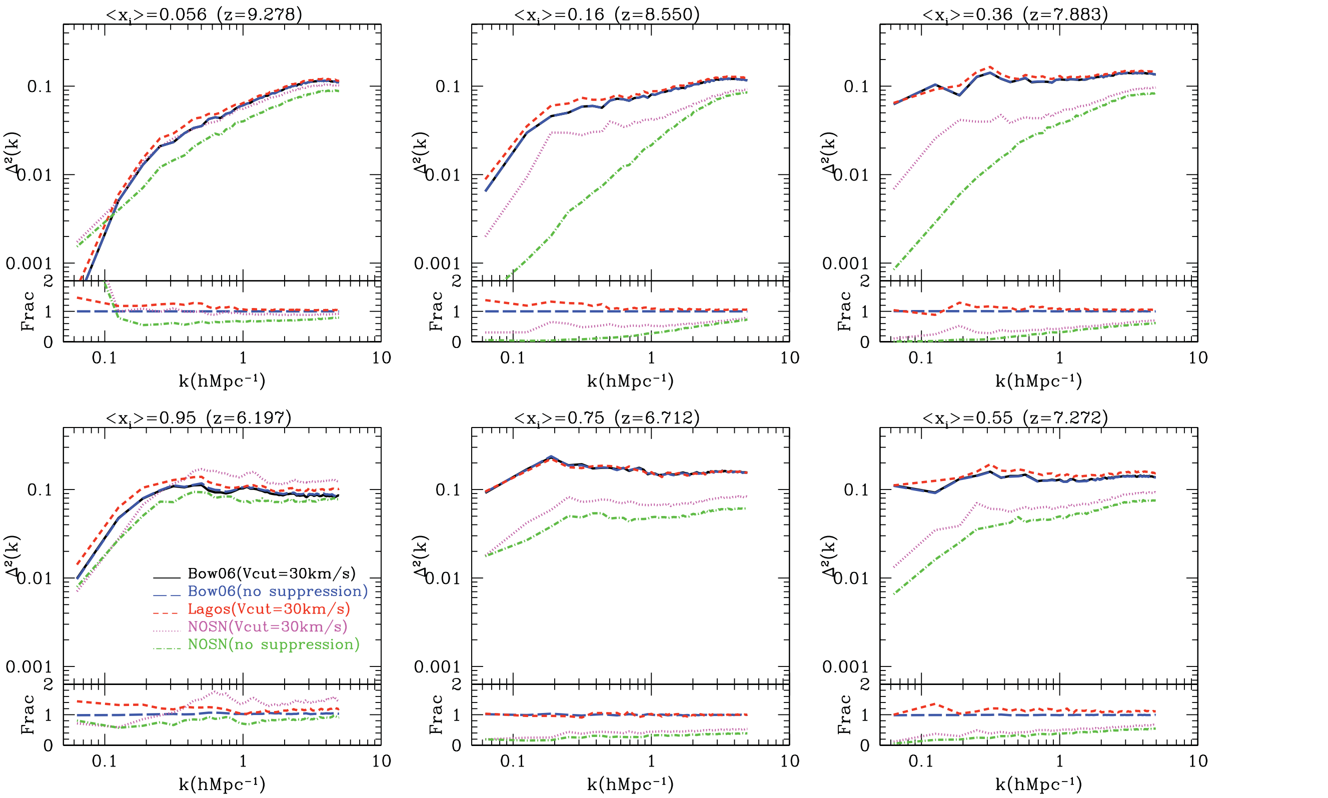

Figure 9. The predicted 21-cm dimensionless power spectra for the models discussed in this paper. Panels are shown for a range of values of $\langle x_i \rangle$ corresponding to different stages of reionization as shown in Figs 2–6. The units of the dimensionless power spectrum are $(28[(1+z)/10]\ \mathrm{mK})^2$. In the lower subpanels we show the ratio of the other models to the Bow06 model.

the difference between the Bow06 and the Bow06 (no suppression) models at any redshifts. There is a small difference between the Bow06 and Lagos models at all redshifts, although the magnitude of difference is smaller than between the Bow06 and NOSN models. There is also a difference between the NOSN and NOSN (no suppression) models. The bottom panels in Fig. 9 show the ratio between the models and the Bow06 model for each redshift.

6.1 Observational implications

Lidz et al. (2008) demonstrated that first-generation low-frequency arrays like the MWA[3] should have sufficient sensitivity to measure the amplitude and slope of the 21-cm power spectrum. To quantify the effect of SN feedback on the power spectrum we therefore compare the amplitude and slope of predicted 21-cm power spectra for the Bow06, NOSN, Bow06 (no suppression), NOSN (no suppression) and Lagos models. In Fig. 10, we plot these values as a function of the $\langle x_i \rangle$ for central wavenumbers of $k_\mathrm{p} = 0.2$ and $0.4\,h^{-1}$ Mpc, corresponding to the range of wavenumbers to be probed by the MWA. There are significant differences in the predicted quantities. For $k_\mathrm{p} = 0.2\,h^{-1}$ Mpc, the inclusion of SN feedback results in fractional changes that are of the order of unity, particularly near the peak of reionization.

Since the ionization fraction is not a direct observable, we plot the progression of a model in the observable plane of power spectrum amplitude versus slope. These are shown for the variant models in Fig. 11, again for the two values of central wavenumber k_p, corresponding to the point on the power spectrum at which we evaluate

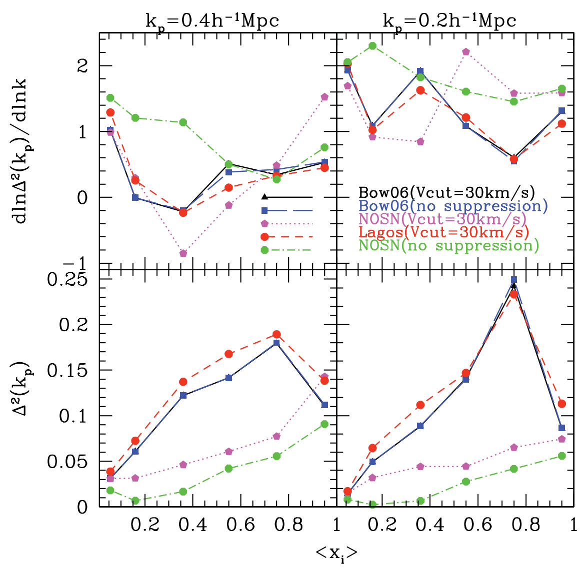

Figure 10. Plots of the evolution in dimensionless 21-cm power spectrum amplitude (lower panels) and slope (upper panels) as a function of ionization fraction $\langle x_i \rangle$. Predictions are shown for models, Bow06 (triangles, black solid line), NOSN (pentagons, violet dotted line), Bow06 (no suppression) (squares, blue long dashed line), Lagos (circles, red dashed line) and NOSN (no suppression) (octagons, green dot dashed line). Results are shown for two central wavenumbers, $k_\mathrm{p} = 0.4\,h^{-1}$ Mpc (left) and $0.2\,h^{-1}$ Mpc (right), corresponding to the point on the power spectrum at which we evaluate the amplitude and gradient.

[3] www.mwa.org

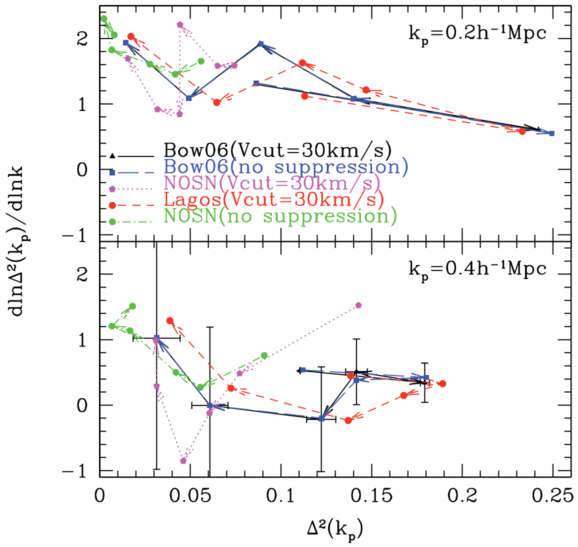

Figure 11. Plots of the loci of points in the parameter space of 21-cm power spectrum amplitude and slope. Loci are shown for each of Bow06 (triangles, black solid line), NOSN (pentagons, violet dotted line), Bow06 (no suppression) (squares, blue long dashed line), Lagos (circles, red dashed line) and NOSN (no suppression) (octagons, green dot dashed line) models. Results are shown for two central wavenumbers, $k_\mathrm{p} = 0.2\,h^{-1}$ Mpc (top) and $0.4\,h^{-1}$ Mpc (bottom), corresponding to the point on the power spectrum at which we evaluate the amplitude and gradient. The error bars for $0.4\,h^{-1}$ Mpc at each point on the Bow06 model correspond to estimates for the MWA (specifically an r^{-2} distribution of 500 antennas) (Lidz et al. 2008) with 1000 h of integration and 6 MHz of bandpass.

the amplitude and gradient. The arrows show the direction from high to low $\langle x_i \rangle$ (from 0.95 to 0.056). The tracks separate according to whether SN feedback is included or not and difference of star formation prescription in the models (the Bow06 and Lagos models). To illustrate the potential for detectability of this difference we also include error bars at each point corresponding to estimates for the MWA (specifically an r^{-2} distribution of 500 antennas) (Lidz et al. 2008) assuming 1000 h integration and 6 MHz bandpasses for wavenumber $k_\mathrm{p} = 0.4\,h^{-1}$Mpc. The figure demonstrates that mid-way through reionization (i.e. at the highest amplitude), the difference between the tracks for models with and without SN feedback could be detected by the MWA, indicating that the strength of SN feedback during the epoch of reionization could be inferred directly from observations of the 21-cm power spectrum.

7 SUMMARY AND CONCLUSIONS

Over the next decade we are likely to see the first measurements of the power spectrum of redshifted 21-cm fluctuations from neutral hydrogen structure during the epoch of reionization. One goal of these experiments will be to learn about the properties of the galaxies that drove the reionization process. It is known that the ionization structure of the IGM, and hence the observed 21-cm power spectrum, will be sensitive to the astrophysical properties of the reionizing galaxies. With this in mind, Barkana (2009) has suggested that analytic models of the power spectrum could be used to determine the astrophysics of the reionizing galaxies, provided that they are tuned to provide a sufficiently precise description through comparison with numerical simulations. However, previous analyses of the structure of reionization and the predicted power spectrum have used very simple prescriptions to relate ionizing luminosity to the underlying dark matter distribution. In this paper, we have made a first attempt to connect the details of the ionization structure and 21-cm power spectrum with realistic models for galaxy formation by combining the GALFORM galaxy formation model implemented within the Millennium-II dark matter simulation with a semi-numerical scheme to describe the resulting ionization structure. While not a true calculation of radiative transfer, semi-numerical models are known to reproduce the main features of the 21-cm power spectrum where reionization is driven by UV ionizing sources. Our model includes a single value for the escape fraction of ionizing photons from galaxies, independent of halo mass. In reality the escape fraction may depend on mass in a way that could be degenerated with the effect of SN feedback.

We find that the details of galaxy formation are reflected in differences in the structure of reionization. As a result, each of the assumed star formation law, radiative feedback and SN feedback are found to affect 21-cm power spectrum predictions. Our main result is that the details of SN feedback are most important in modifying H II region evolution, and hence the slope and amplitude of the 21-cm power spectrum. We find that photoionization feedback also affects H II region evolution but only in the absence of SN feedback. Thus, unless SN feedback is ineffective in high-redshift galaxies, the reionization process is not self-regulating as has been argued previously (e.g. Iliev et al. 2007). This finding is consistent with the work of Raičević et al. (2011) who studied the photon budget in the context of the global evolution of reionization. We find that measurements of the amplitude and slope of the 21-cm power spectrum would be sufficient to determine the level at which SN feedback operated in high-redshift galaxies.

In this work we have concentrated on the effects of SN and radiative feedback which are relevant to the galaxies thought to dominate reionization and are accessible to semi-analytic models implemented within the Millennium-II Simulation, and we have restricted ourselves to the assumption that the escape fraction is not mass dependent. This study illustrates the important role that semi-analytic models can play in realistic simulation of the connection between ionization structure and the properties of the galactic sources responsible for reionization. Our paper is the first step in a programme to determine how redshifted 21-cm observations can be used to probe astrophysics of reionization.

ACKNOWLEDGMENTS

H-SK is supported by a Super-Science Fellowship from the Australian Research Council. The Centre for All-sky Astrophysics is an Australian Research Council Centre of Excellence, funded by grant CE11E0090. This work was supported in part by the Science and Technology Facilities Council rolling grant to the ICC. The Millennium-II Simulation was carried out by the Virgo Consortium at the supercomputer centre of the Max Planck Society in Garching. Calculations for this paper were partly performed on the ICC Cosmology Machine, which is part of the DiRAC Facility jointly funded by STFC, the Large Facilities Capital Fund of BIS and Durham University.

REFERENCES

Barkana R., 2009, MNRAS, 397, 1454
Barkana R., Loeb A., 2005, ApJ, 624, L65
Baugh C. M., 2006, Rep. Prog. Phys., 69, 3101
Baugh C. M., Lacey C. G., Frenk C. S., Granato G. L., Silva L., Bressan A., Benson A. J., Cole S., 2005, MNRAS, 356, 1191

Benson A. J., Nusser A., Sugiyama N., Lacey C. G., 2001, MNRAS, 320, 153
Benson A. J., Lacey C. G., Baugh C. M., Cole S., Frenk C. S., 2002, MNRAS, 333, 156
Benson A. J., Sugiyama N., Nusser A., Lacey C. G., 2006, MNRAS, 369, 1055
Blanton M. R. et al., 2001, AJ, 121, 2358
Bond J. R., Myers S. T., 1996, ApJS, 103, 1
Bouwens R. J., Illingworth G. D., Franx M., Ford H., 2007, ApJ, 670, 928
Bouwens R. J. et al., 2010, ApJ, 709, L133
Bouwens R. J. et al., 2011, Nat, 469, 504
Bower R. G., Benson A. J., Malbon R., Helly J. C., Frenk C. S., Baugh C. M., Cole S., Lacey C. G., 2006, MNRAS, 370, 645
Boylan-Kolchin M., Springel V., White S. D. M., Jenkins A., Lemson G., 2009, MNRAS, 398, 1150
Ciardi B., Stoehr F., White S. D. M., 2003, MNRAS, 343, 1101
Cole S., Lacey C. G., Baugh C. M., Frenk C. S., 2000, MNRAS, 319, 168
Crain R. A. et al., 2009, MNRAS, 399, 1773
Croft R. A. C., Altay G., 2008, MNRAS, 388, 1501
Dijkstra M., Haiman Z., Rees M. J., Weinberg D. H., 2004, ApJ, 601, 666
Efstathiou G., 1992, MNRAS, 256, 43P
Furlanetto S. R., Zaldarriaga M., Hernquist L., 2004a, ApJ, 613, 1
Furlanetto S. R., Zaldarriaga M., Hernquist L., 2004b, ApJ, 613, 16
Furlanetto S., Oh S. P., Briggs F., 2006, Phys. Rep., 433, 181
Geil P. M., Wyithe J. S. B., 2008, MNRAS, 386, 1683
Gnedin N. Y., 2000, ApJ, 535, 530
Hoeft M., Yepes G., Gottlöber S., Springel V., 2006, MNRAS, 371, 401
Iliev I. T., Mellema G., Shapiro P. R., Pen U.-L., 2007, MNRAS, 376, 534
Iliev I. T., Mellema G., Pen U.-L., Bond J. R., Shapiro P. R., 2008, MNRAS, 384, 863
Kim H.-S., Baugh C. M., Benson A. J., Cole S., Frenk C. S., Lacey C. G., Power C., Schneider M., 2011, MNRAS, 414, 2367
Lacey C. G., Baugh C. M., Frenk C. S., Benson A. J., 2011, MNRAS, 412, 1828
Lagos C. d. P., Bayet E., Baugh C. M., Lacey C. G., Bell T., Fanidakis N., Geach J., 2012, MNRAS, 426, 2142
Lee K.-G., Cen R., Gott J. R. I., Trac H., 2008, ApJ, 675, 8
Lidz A., Zahn O., McQuinn M., Zaldarriaga M., Hernquist L., 2008, ApJ, 680, 962
Mao Y., Shapiro P. R., Mellema G., Iliev I. T., Koda J., Ahn K., 2012, MNRAS, 422, 926
McLure R. J., Cirasuolo M., Dunlop J. S., Foucaud S., Almaini O., 2009, MNRAS, 395, 2196
McLure R. J., Dunlop J. S., Cirasuolo M., Koekemoer A. M., Sabbi E., Stark D. P., Targett T. A., Ellis R. S., 2010, MNRAS, 403, 960
McQuinn M., Lidz A., Zahn O., Dutta S., Hernquist L., Zaldarriaga M., 2007, MNRAS, 377, 1043
Mellema G., Iliev I. T., Pen U.-L., Shapiro P. R., 2006, MNRAS, 372, 679
Merson A. I. et al., 2012, preprint (arXiv e-prints)
Mesinger A., Dijkstra M., 2008, MNRAS, 390, 1071
Mesinger A., Furlanetto S., 2007, ApJ, 669, 663
Norberg P. et al., 2002, MNRAS, 336, 907
Oesch P. A. et al., 2010, ApJ, 709, L16
Okamoto T., Gao L., Theuns T., 2008, MNRAS, 390, 920
Ouchi M. et al., 2010, ApJ, 723, 869
Raičević M., Theuns T., Lacey C., 2011, MNRAS, 410, 775
Santos M. G., Amblard A., Pritchard J., Trac H., Cen R., Cooray A., 2008, ApJ, 689, 1
Shin M.-S., Trac H., Cen R., 2008, ApJ, 681, 756
Sokasian A., Abel T., Hernquist L., Springel V., 2003, MNRAS, 344, 607
Trac H., Cen R., 2007, ApJ, 671, 1
Trac H., Cen R., Loeb A., 2008, ApJ, 689, L81
Wyithe S., Loeb A., 2012, preprint (arXiv e-prints)
Wyithe J. S. B., Morales M. F., 2007, MNRAS, 379, 1647
Zahn O., Lidz A., McQuinn M., Dutta S., Hernquist L., Zaldarriaga M., Furlanetto S. R., 2007, ApJ, 654, 12

APPENDIX A: MODELLING SPATIALLY DEPENDENT REIONIZATION FEEDBACK IN GALFORM

This appendix describes how spatially dependent reionization feedback is implemented in GALFORM for the calculations in this paper. The steps in the modelling are as follows.

(1) We first run GALFORM at high redshift (from redshift∼20) to find the first resolved H II region using the scheme described in Section 3.1. We assume $(1 + F_c)/f_{esc} = 1$ for this step.

(2) For snapshots at redshifts where the first H II region is identified, we then find those galaxies which are inside H II regions and subject to radiative feedback through regulation of cooling processes (i.e. galaxies with $V < V_{cut}$).

(3) A table listing these galaxies is generated for each snapshot. This table identifies which galaxies should have star formation regulated by radiative feedback during subsequent evolution up to the next snapshot redshift.

(4) GALFORM is then run to the next redshift snapshot, including regulation of cooling processes in the galaxies identified in the table at step (3).

(5) Steps (2) to (4) are then repeated for all snapshots down to redshift 6 where reionization is finished.

This paper has been typeset from a TEX/LATEX file prepared by the author.